JOURNAL OF SPACECRAFT AND ROCKETS
Vol. 29, No. 6, November–December 1992

Natural Convection with Thermocapillary and Gravity Modulation Effects in Low-Gravity Environments

T. C. Jue* and B. Ramaswamy†
Rice University, Houston, Texas 77251

The characteristics of natural convection in a rectangular cavity with simultaneous thermocapillary and gravity modulation effects have been studied numerically. Because of the practical applications, the simulation focuses on low-Prandtl-number and zero-gravity situations. The two-dimensional, time-dependent Navier-Stokes and energy equations are numerically integrated by a semi-implicit time-splitting method. For a specific Rayleigh number, Prandtl number, and Marangoni number, the problem is investigated for different modulation frequencies and directions. From the results, it can be concluded that thermocapillarity seriously affected the flowfield, especially in high-frequency cases.

Nomenclature

Ar = aspect ratio (H/L)
F_m = mean value amplitude
H = height of the cavity, m
k = thermal conductivity, J/m · °C · s
L = width of the cavity, m
p = dimensionless pressure
p = finite element variable vector for p
Ma = Marangoni number
Nu = Nusselt number, $\int_0^1 -\frac{\partial T}{\partial y}\,dx$
Pr = Prandtl number
Ra = Rayleigh number
S = source term
T = dimensional temperature, K
t = dimensionless time
u, v = dimensionless velocity components in x and y directions
u = finite element variable vector for u and v
(x, y) = Cartesian coordinates
α = thermal diffusivity, m^2/s
β = thermal expansion coefficient, K^{-1}
η = dimensionless amplitude
θ = dimensionless temperature
μ = viscosity coefficient, kg/ms
ν = kinematic viscosity coefficient, m^2/s
ρ = density, kg/m^3
σ = surface tension, N/m
ϕ = phase angle
Ψ = stream function
Ω = bounded domain in R^2
ω = dimensionless frequency

Superscripts

* = dimensional value
~ = intermediate value

Subscripts

c = cold wall
h = hot wall
m = mean value
1 = the source term in the x direction
2 = the source term in the y direction

Received Nov. 18, 1991; presented as Paper 92-0667 at the AIAA 30th Aerospace Sciences Meeting, Reno, NV, Jan.6–9, 1992; revision received April 9, 1992; accepted for publication May 1, 1992.

*Graduate Student, Dept. of Mechanical Engineering and Materials Science.
†Assistant Professor, Dept. of Mechanical Engineering and Materials Science. Senior Member AIAA.

I. Introduction

NATURAL convection phenomena is known to play a dominant role in material processing and in crystal growth. For example, it increases the crystal growth rate which is good for the process by enhancing the overall transport rate. Contrarily, it adversely affects the local growth condition by creating nonuniform mass flux. Because of these reasons, the understanding and control of the natural convection is an important factor in improving material properties. As is well known, the natural convection flow is much weaker in low-gravity conditions than in normal-gravity state. Therefore, a lot of microgravity environments are developed or applied to do the crystal-growth experiments. However, in microgravity environments, variation of surface tension on the gas-liquid interface resulting from temperature gradients along the free surface is another important source to create bulk fluid motions and temperature fields, which are termed thermocapillary convection. In addition, when gravity becomes weaker, other disturbances will be sources to change the fluid flow, such as: spacecraft maneuvers, crew motions, and mechanical vibrations in the space lab, and as such must be accepted as part of the natural environment, and their effects be taken into account. The consideration of surface tension and gravity modulation (g-jitter) effects in natural convection are inevitable for studying the material processing or crystal-growth process in microgravity environments. Understanding the heat transfer mechanisms and fluid-flow characteristics of such problems is an important step in developing new innovative techniques and producing high-quality materials.

In previous literature, most of the research was conducted in natural convection with thermocapillary effect in normal-gravity condition. Bergman and Ramadhyani[1] studied the physical phenomena in a two-dimensional cavity by the SIMPLER method for different Rayleigh numbers. Bergman and Keller[2] applied the same algorithm to investigate this physical problem for liquid metal materials. A scale consideration was made by Carpenter and Homsy[3] to get a systematic understanding of the physical phenomena. Shyy and Chen[4] used the finite volume method to explore the effect of the mesh sizes on this problem. Recently, Keller and Bergman,[5] Shyy and Chen,[6] and Lan and Kou[7] considered the thermocapillary effect in the material solidification process. These studies concentrated primarily on the steady-state governing equations. Jue et al.[8] carried out the transient formulation for this problem in their recent research.[8] Incropera et al.[9] and Lacroix[10] used a transient formulation in a solidification problem with

the thermocapillary effect and made it possible to understand the flow phenomena. The natural convection flow influenced by gravity modulation has been studied by stability analysis and by numerical simulations. Gresho and Sani[11] considered this problem using linearized equations of motion coupled with the nonlinear energy equation which resulted in many important conclusions. Kamotani et al.[12] applied a perturbation method analyzing horizontal gravity modulation phenomena. Recently, Biringen and Danabasoglu,[13] using a finite difference method, widely studied the gravity modulation effects in a rectangular cavity under normal-gravity and zero-gravity conditions. However, none of these studies dealt with the combined thermocapillary and gravity modulation effects in microgravity environments which is considered in the present work.

We consider a two-dimensional cavity with aspect ratio 0.5. Instead of time-averaged, steady-state equations, the full Navier-Stokes equations are integrated through the transient phase. Computation of convective flow with gravity modulation in cavities are investigated with and without thermocapillary effect for comparison purposes. A parametric study is conducted to determine the critical modulation frequency for both vertical and horizontal modulations.

II. Problem Formulation

In this problem, the fluid is considered to be viscous, incompressible, and the flow is laminar. The transient incompress-

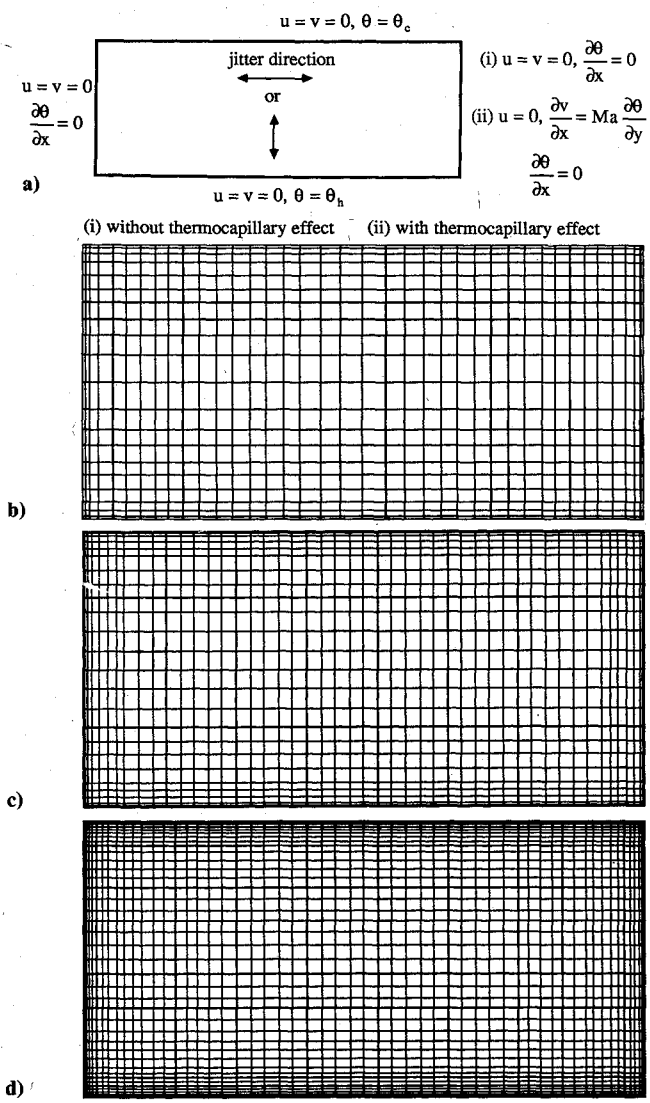

Fig. 1 Natural convection with thermocapillary and gravity modulation effects: a) problem definition; b) nonuniform mesh (20 × 38); c) nonuniform mesh (24 × 48); and d) nonuniform mesh (38 × 56).

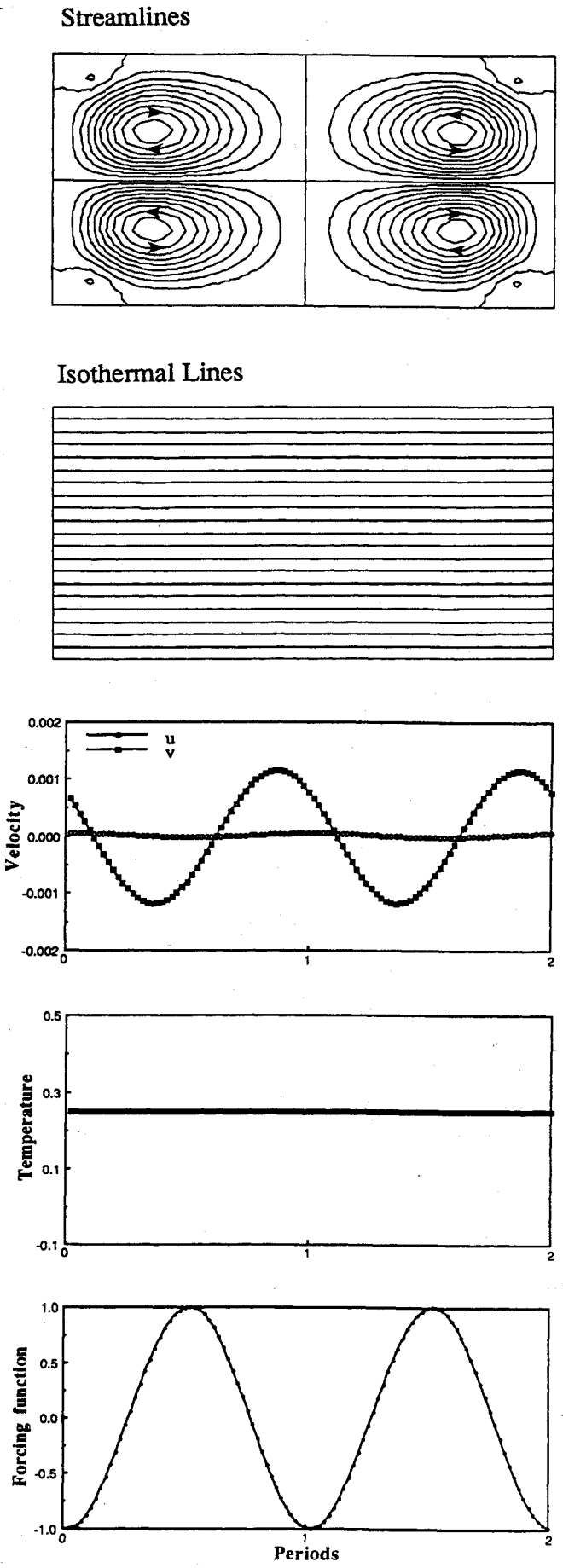

Fig. 2 Time-averaged results for $Ra = 1.771 \times 10^5$, $Pr = 0.007$, $\eta = 1$, $\omega = 4543$, $Ar = 0.5$, and zero g (vertical jitter).

ible Navier-Stokes and energy equations are considered with the Boussinesq assumption for the density. The geometry of the flow domain is considered to be a two-dimensional rectangular cavity with aspect ratio $Ar = 0.5$. For the calculations without thermocapillary effect, the walls of the cavity are solid walls; but for the calculations with thermocapillary effect, the right-hand boundary of the cavity is considered as a free surface. All of the variables are nondimensionalized following the procedures as given in Bergman's research[1]:

$$x = x^*/H$$

$$y = y^*/H$$

$$u = u^*/(\alpha/H)$$

$$v = v^*/(\alpha/H)$$

$$p = p^*/(\rho\alpha^2/H^2)$$

$$\theta = (T - T_m)/(T_h - T_c)$$

and

$$t = t^*/(H^2/\alpha)$$

Subject to these assumptions, the dimensionless governing equations for the system are as follows:

Continuity:

$$\frac{\partial u}{\partial x} + \frac{\partial v}{\partial y} = 0, \quad \text{in } \Omega \tag{1}$$

x Momentum:

$$\frac{\partial u}{\partial t} + \left(u\frac{\partial u}{\partial x} + v\frac{\partial u}{\partial y}\right) = -\frac{\partial p}{\partial x} + Pr\left(\frac{\partial^2 u}{\partial x^2} + \frac{\partial^2 u}{\partial y^2}\right) + S_1 \quad \text{in } \Omega \tag{2}$$

y Momentum:

$$\frac{\partial v}{\partial t} + \left(u\frac{\partial v}{\partial x} + v\frac{\partial v}{\partial y}\right) = -\frac{\partial p}{\partial y} + Pr\left(\frac{\partial^2 v}{\partial x^2} + \frac{\partial^2 v}{\partial y^2}\right) + S_2 \quad \text{in } \Omega \tag{3}$$

Energy:

$$\frac{\partial \theta}{\partial t} + \left(u\frac{\partial \theta}{\partial x} + v\frac{\partial \theta}{\partial y}\right) = \left(\frac{\partial^2 \theta}{\partial x^2} + \frac{\partial^2 \theta}{\partial y^2}\right), \quad \text{in } \Omega \tag{4}$$

where

$$S_1 = S_2 = RaPr\theta[F_m + \eta\cos(\omega t + \phi)] \tag{5}$$

In Eq. (5), F_m represents the constant- (mean-) gravity level such that $F_m = 0$ implies zero g. Also, η is the amplitude of the oscillatory part of the source term, and ϕ stands for random phase angle, which is set to zero for sinusoidal oscillation. The dimensionless parameters included in this formulation are

$$Ra = g\beta\Delta TH^3/\nu\alpha \tag{6}$$

$$Pr = \nu/\alpha = \mu c_p/k \tag{7}$$

$$Ma = \frac{\partial\sigma}{\partial T}\frac{\Delta TH}{\mu\alpha} \tag{8}$$

and the cavity aspect ratio H/L. The Marangoni number is an index of the relative strengths of surface tension and viscous forces.

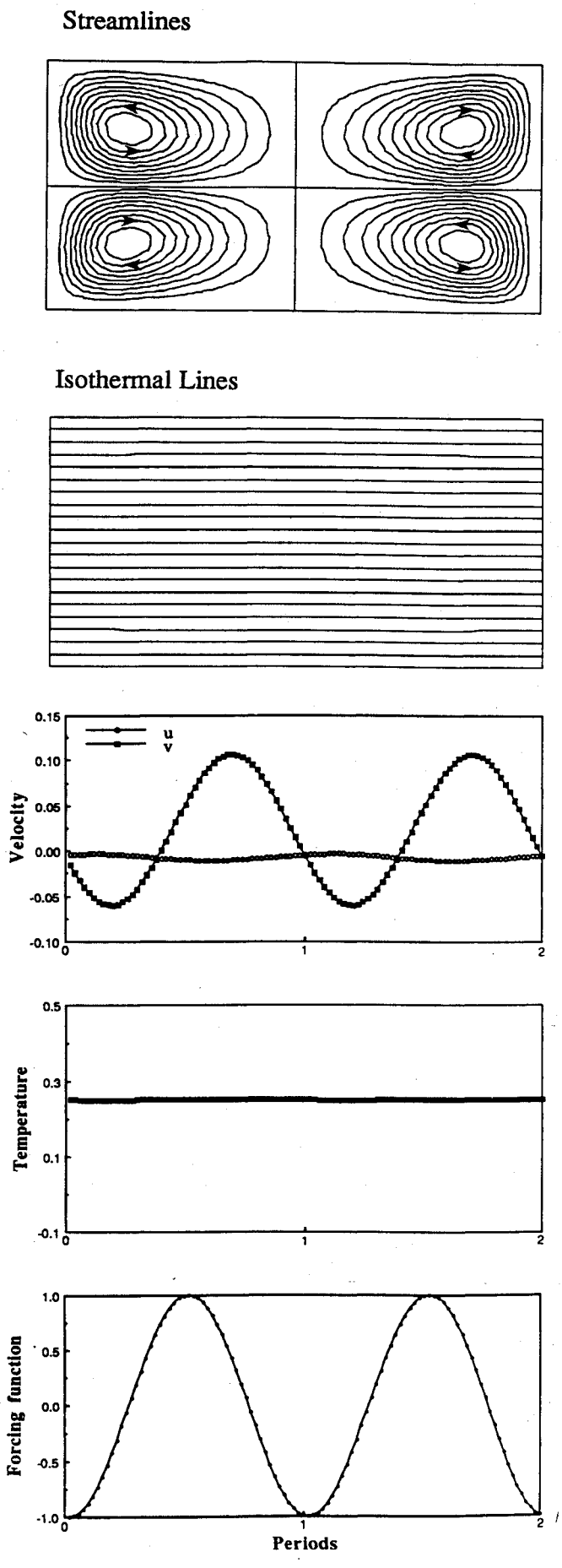

Fig. 3 Time-averaged results for $Ra = 1.771 \times 10^5$, $Pr = 0.007$, $\eta = 1$, $\omega = 45.5$, $Ar = 0.5$, and zero g (vertical jitter).

The hydrodynamic and thermal boundary conditions on the fixed surfaces are specified as (see Fig. 1a)

$$u = v = 0, \qquad \theta = \theta_h = 0.5, \qquad y = 0 \tag{9}$$

$$u = v = 0, \qquad \theta = \theta_c = -0.5, \qquad y = Ar \tag{10}$$

$$u = v = 0, \qquad \frac{\partial \theta}{\partial x} = 0, \qquad x = 0 \tag{11}$$

The boundary conditions at $x = 1$ for the two cases considered in this study are as follows:

Case 1 (without thermocapillary effect):

$$u = v = 0, \qquad \frac{\partial \theta}{\partial x} = 0 \tag{12}$$

Case 2 (with thermocapillary effect):

$$u = 0, \quad \frac{\partial v}{\partial x} = Ma \frac{\partial \theta}{\partial y}, \quad v = 0, \quad \frac{\partial \theta}{\partial x} = 0 \tag{13}$$

The free surface of the liquid has been assumed to be perfectly flat, i.e., the contact angle is 90 deg. Equation (13) reveals that the temperature gradients along the free surface result in an effective shear if the liquid surface tension varies with the fluid temperature. The shear stress, in turn, drives thermocapillary convection.

III. Method of Solution

We presented the finite element formulation used in detail in our previous work.[14,15] Here we summarize briefly the major ingredients of the formulation and resulting equations, and point out some important features regarding the practical application of these equations. The Galerkin finite element method is used for spatial discretization. The dependent variables u, v, p, and θ are represented in four-node bilinear quadrilateral shape functions. A semi-implicit time-splitting scheme is used for the temporal discretization. The solution procedure of the system is accomplished by splitting the equation into parts: the nonlinear terms are advanced by the explicit second-order Adams-Bashford scheme, and the linear diffusion terms are advanced by an implicit Euler scheme.

At the first step, a set of equations is solved without inclusion of the pressure term:

$$\frac{\tilde{u}^{n+1} - u^n}{\Delta t} = -[\tfrac{3}{2}(u \cdot \nabla u)^n - \tfrac{1}{2}(u \cdot \nabla u)^{n-1}] + \nabla \cdot \nabla u^{n+1} + RaPr\theta^n \tag{14}$$

After this intermediate step, the flowfield is not incompressible. The pressure is then used to enforce incompressibility. A Poisson equation for the pressure is obtained by taking the divergence of the momentum equation. Assume that u^n is incompressible, the equation for the pressure is:

$$\nabla^2 p^{n+1} = \nabla \cdot \frac{\tilde{u}^{n+1}}{\Delta t} \tag{15}$$

Using the intermediate velocity $\tilde{u}$ and pressure p, we correct the final velocity as:

$$u^{n+1} = \tilde{u}^{n+1} - \Delta t \nabla p^{n+1} \tag{16}$$

The similar procedure for the intermediate velocity is used for the temperature calculation θ^{n+1} by solving the energy equation after obtaining the final velocity u^{n+1}.

$$\frac{\theta^{n+1} - \theta^n}{\Delta t} = -[\tfrac{3}{2}(u \cdot \nabla \theta)^n - \tfrac{1}{2}(u \cdot \nabla \theta)^{n-1}] + \nabla \cdot \nabla \theta^{n+1} \tag{17}$$

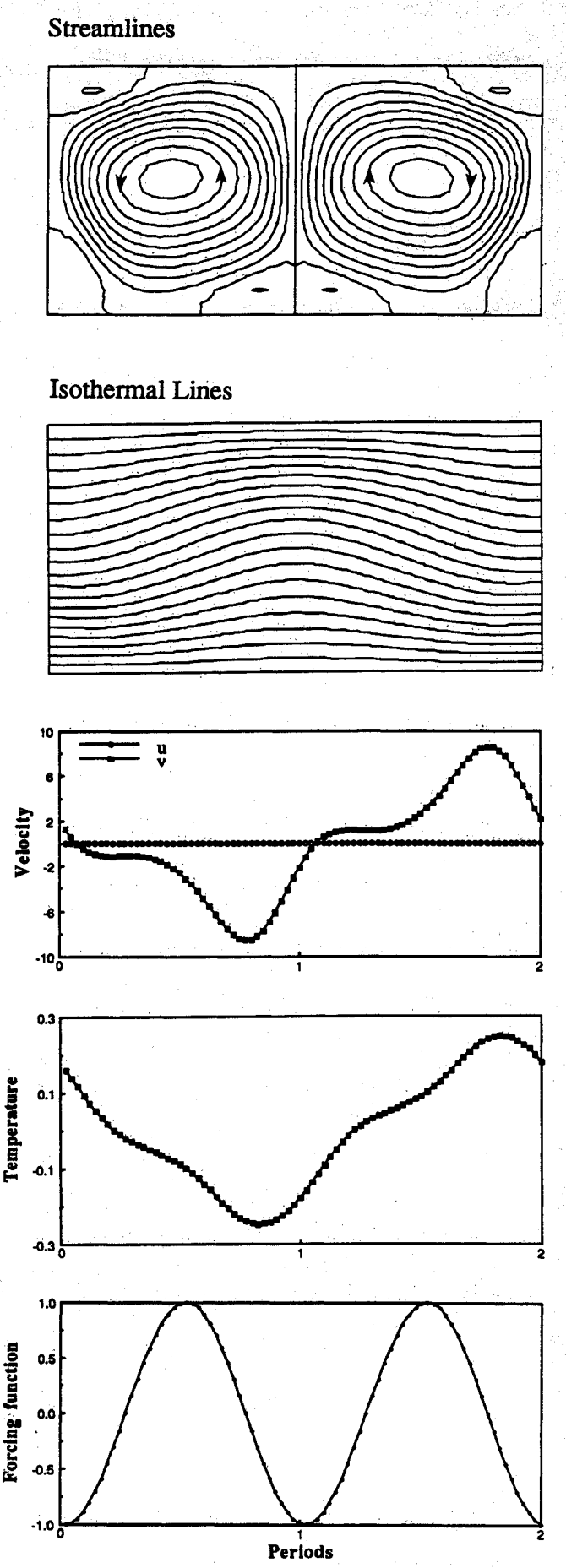

Fig. 4 Time-averaged results for $Ra = 1.771 \times 10^5$, $Pr = 0.007$, $\eta = 1$, $\omega = 20$, $Ar = 0.5$, and zero g (vertical jitter).

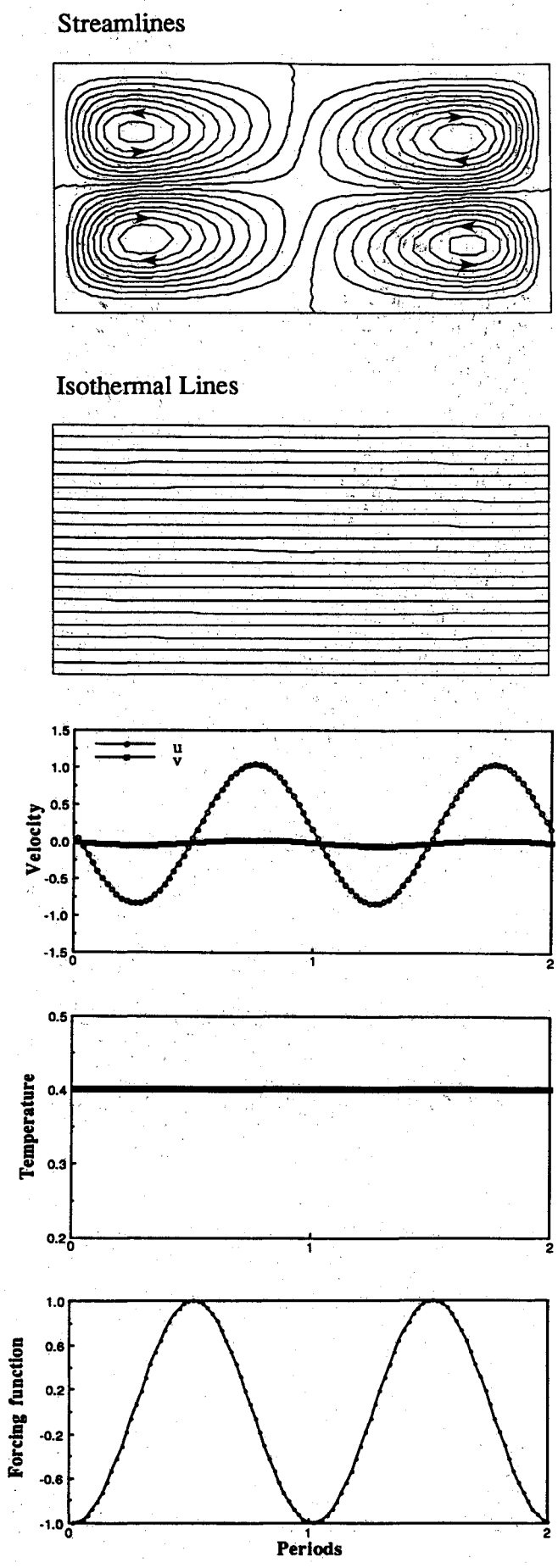

Fig. 5 Time-averaged results for $Ra = 1.771 \times 10^5$, $Pr = 0.007$, $\eta = 1$, $\omega = 450$, $Ar = 0.5$, and zero g (horizontal jitter).

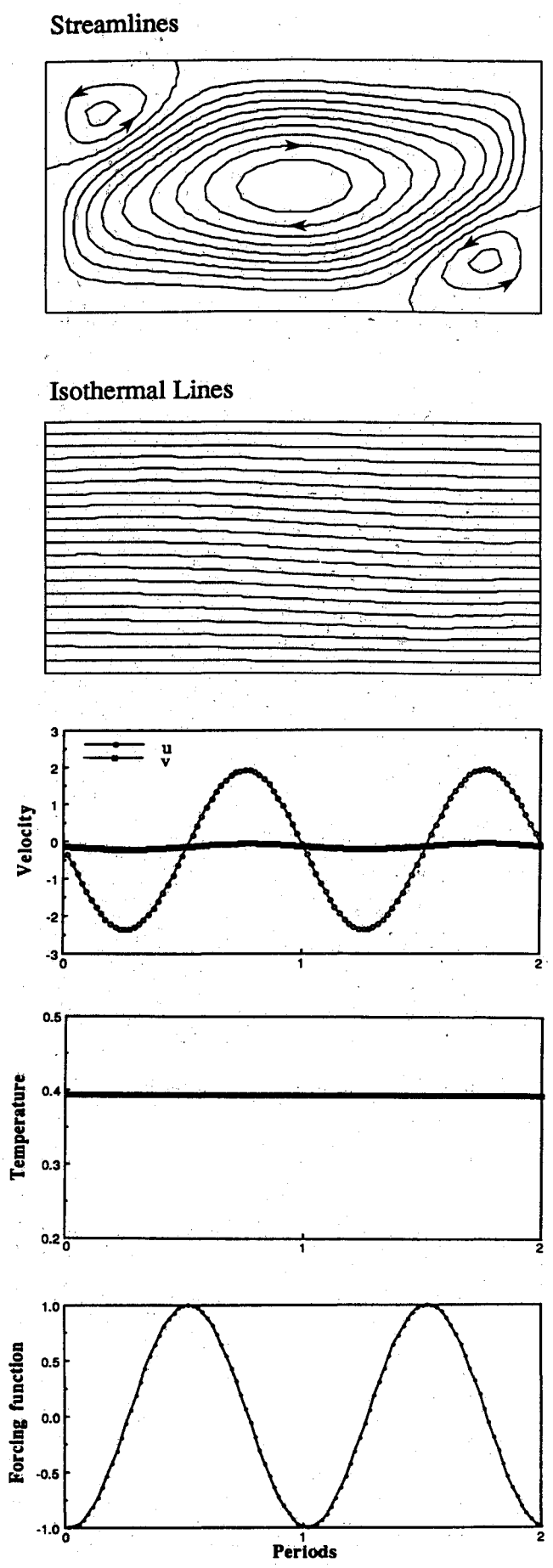

Fig. 6 Time-averaged results for $Ra = 1.771 \times 10^5$, $Pr = 0.007$, $\eta = 1$, $\omega = 200$, $Ar = 0.5$, and zero g (horizontal jitter).

Because of the explicit treatment for the nonlinear terms in this solution procedure, the coefficient matrix of the system equations remains constant and symmetric. By taking advantage of this characteristic, the computation time and storage are economical. In addition, the application of implicit treatment for the viscous terms may obviously save computation time by choosing a bigger time increment compared to the fully explicit algorithm. Owing to these benefits, the present method appears to be reasonably efficient and robust, converging over a wide range of physical parameters from a zero initial guess.

IV. Results and Discussion

In the first part of this section, we provide the nonlinear analysis of the zero-g cases without thermocapillary effect. The second part contains the results with thermocapillary effect. A study of the effect of mesh on the results is listed in Table 1. Because of the computational cost and accuracy considerations, by observing Table 1, a 20×40 uniform mesh is used for the first part of the calculations. For the calculations of the second part, a 24×48 nonuniform mesh (see Fig. 1c) is used to provide fine grid spacing near the boundaries of the cavity. Coarse spacing near the center followed the considerations for the singularity induced by thermocapillary flow on the right-hand surface provided by Zehr et al.[16]

A. Results Without Thermocapillary Effect

In this subsection, the focus is put on the effects of gravity modulation and direction in the thermal-driven cavity flow without thermocapillary effect. According to the practical applications, a low-Prandtl-number material, such as liquid metal, is a typical sample for investigation about the flowfield and heat transfer in zero-gravity environments. In these calculations, we set the thermal diffusivity $k = 2.2 \times 10^{-5}$ m^2/s, kinematic viscosity $\nu = 1.54 \times 10^{-7}$ m^2/s, and thermal expansion $\beta = 10^{-4}$ K^{-1} as the material properties. When the flowfield exists in a g-jitter environment with maximum amplitude[17] 10^{-3} g, characteristic length 0.18 m, and maximum temperature difference 100 K, we calculate the Prandtl number $Pr = 7 \times 10^{-3}$ and Rayleigh number $Ra = 1.771 \times 10^5$ by applying these values and the material properties. The purpose of this study is to investigate the modulation direction and the influence of oscillation frequencies; and, therefore, the Prandtl and Rayleigh numbers are fixed to the given values for all of the calculations in this section to make the comparison easy.

In the first set of computations, the cavity was subjected to vertical gravity modulation along the direction of the temperature gradient and a different modulation frequency was chosen for each case to find the critical value for the heat transfer mechanism changing from conduction to convection. We started with a high frequency of $\omega = 4543$ and chose $\eta = 1$. That means the maximum modulation amplitude 10^{-3} g is included in the Rayleigh number calculation. The calculated results are shown for this case in Fig. 2. The streamlines include four primary cells (lower-left and upper-right circulations in counterclockwise direction, and lower-right and upper-left circulations in clockwise direction) with a counter-rotating small eddy at each corner of the cavity; and the temperature contours display primarily a conductive pattern. A point data history corresponding to the fluid particle variation along the time axis is obtained at point (0.5, 0.25) for all of the calculations. Because of small gravity modulation, the velocity-time history demonstrates a small variation and the temperature-time history is close to a straight line. All of the point data history explains that this is a synchronous response case, which means one forcing cycle corresponds to one velocity or temperature cycle.

In the subsequent case presented here, the ω is reduced to 45.5 to investigate the effect of the frequency. Figure 3 includes the time-averaged streamlines, isotherms, and the point data history. The streamlines show the existence of only four primary circulations and their rotating directions are opposite to the case where $\omega = 4543$. That means the small circulations existing at corners in Fig. 2a become bigger in size and dominate the flow domain. The time history of velocity is a synchronous response and the flowfield is unexcited. The heat transfer mechanism is still conductive. However, the reduction of frequency has increased the strength of circulation resulting in larger variation in the velocity-time history when compared to the results at $\omega = 4543$.

When the frequency is reduced to 20, the physical phenomena display a dramatic change where the four-circulation balance status as shown in Figs. 2 and 3 is broken into two main cells, four small eddies at the corners and two other small eddies at the vertical centerline near the wall area. The flowfield is excited to strong convection phenomena which is clearly demonstrated by looking at the convective pattern in the temperature distributions (see Fig. 4). In fact, we can find other details from the point data history which show that the velocity and temperature vary subharmonically with the forcing function, i.e., two forcing cycles corresponding to one velocity or temperature cycle. The time-averaged results shown here are obtained by averaging the data of one forcing cycle corresponding to half of the velocity cycle or temperature cycle. If we did the average by using the other half-velocity cycle, the contours would be the same pattern but the eddies would appear at opposite locations symmetric to the horizontal centerline with the current results displayed in Fig. 4.

According to the preceding results, the first two cases are unexcited examples where the flow is a synchronous response, but the third is an excited and subharmonic response case. As the frequency is reduced further, the strength of the circulation is increased. The critical frequency range for flow transferring from a synchronous characteristic to a subharmonic characteristic is $\omega = 20$.

The second set of computations in this subsection is focused on the horizontal gravity modulation effect which means the

Table 1 Extrema stream function values for different frequencies in zero-g gravity modulation environment

Modulation direction	ω	Without thermocapillarity	With thermocapillarity, $Ma = -100$	With thermocapillarity, $Ma = -1000$
Vertical modulation	4543	0.00000436	0.390	—
	200	0.0007	—	—
	45.5	0.0244	0.220	0.600
	20	0.627	0.770	—
Horizontal modulation	450	0.032	0.478	1.570
	300	0.071	—	—
	200	0.245	0.684	1.950
	100	2.820	—	—
	85	3.340	3.712	4.650
	40	4.290	—	—

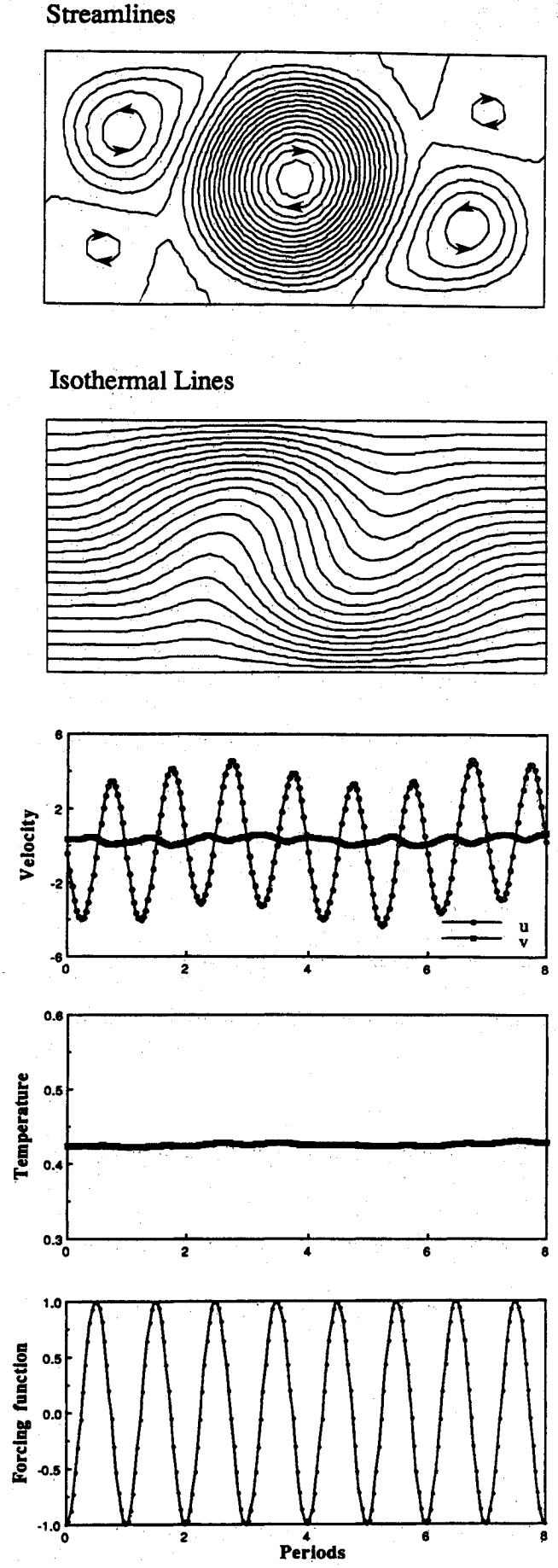

Fig. 7 Time-averaged results for $Ra = 1.771 \times 10^5$, $Pr = 0.007$, $\eta = 1$, $\omega = 85$, $Ar = 0.5$, and zero g (horizontal jitter).

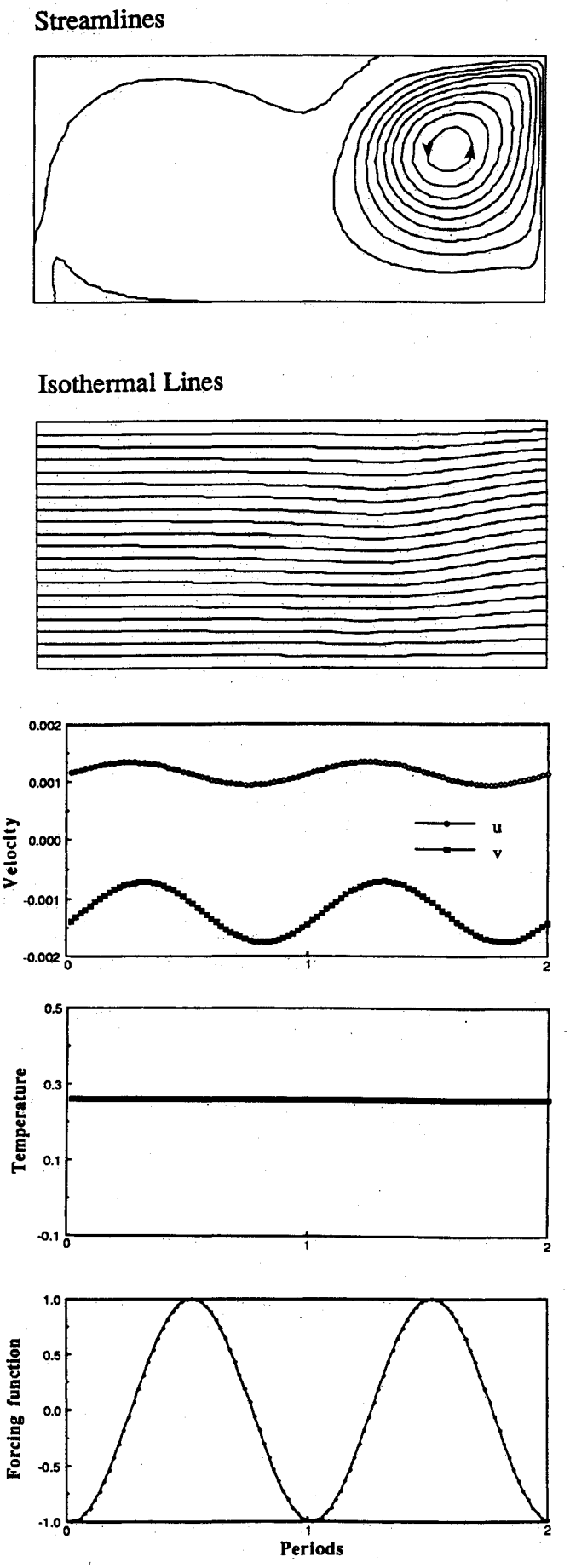

Fig. 8 Time-averaged results for $Ra = 1.771 \times 10^5$, $Ma = -10^2$, $Pr = 0.007$, $\eta = 1$, $\omega = 4543$, $Ar = 0.5$, and zero g (vertical jitter).

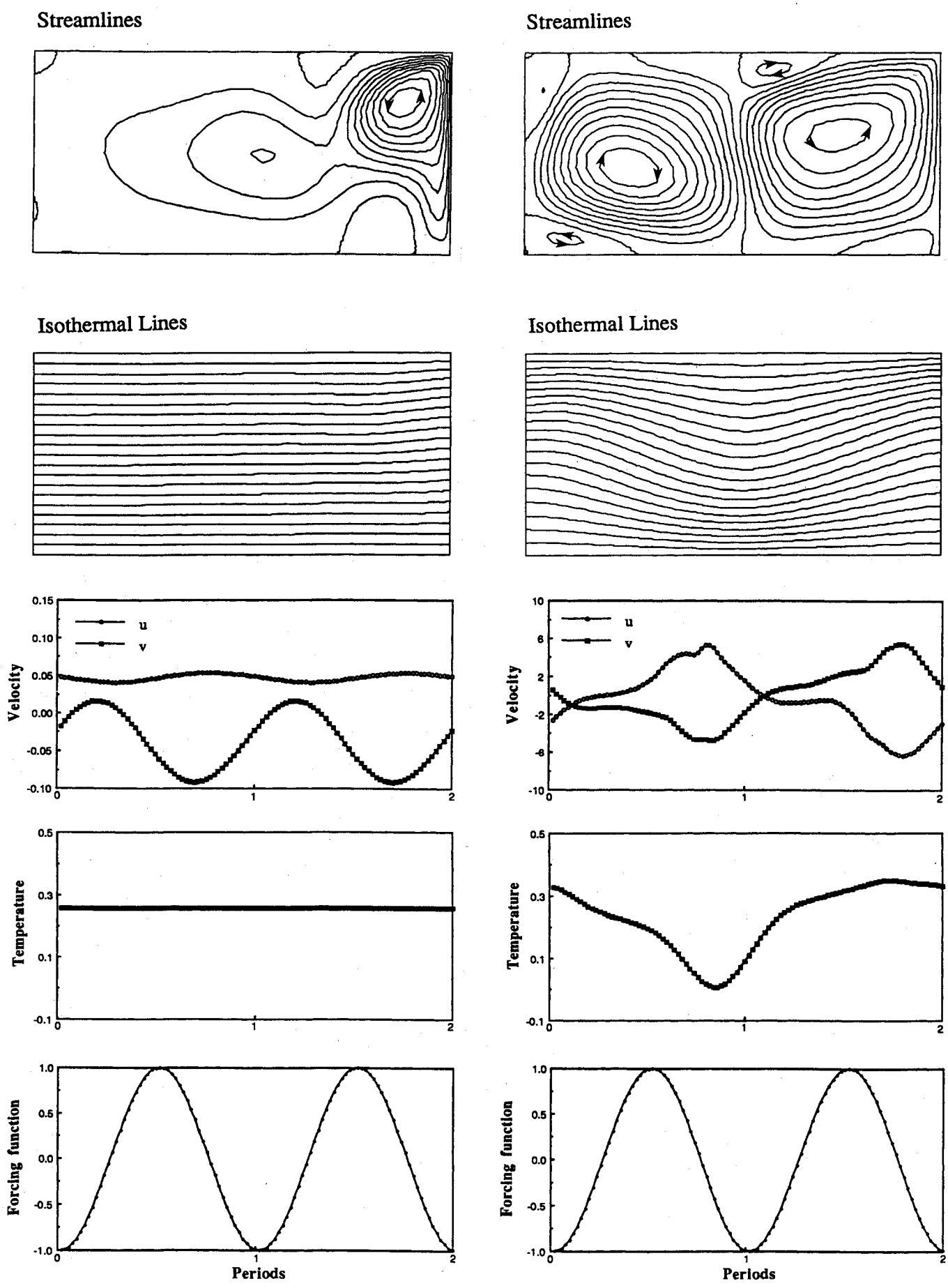

Fig. 9 Time-averaged results for $Ra = 1.771 \times 10^5$, $Ma = -10^2$, $Pr = 0.007$, $\eta = 1$, $\omega = 45.5$, $Ar = 0.5$, and zero g (vertical jitter).

Fig. 10 Time-averaged results for $Ra = 1.771 \times 10^5$, $Ma = -10^2$, $Pr = 0.007$, $\eta = 1$, $\omega = 20$, $Ar = 0.5$, and zero g (vertical jitter).

modulation direction is perpendicular to the temperature gradient direction. As is known, the flow is more sensitive to the horizontal modulation effect.[12] Following the previous procedure, the high-frequency case was studied first to investigate the excitation frequency and the other parameters were kept the same as the vertical modulation cases. We started with $\omega = 450$ and the results are listed in Fig. 5. There are four counter-rotating circulations in the fluid domain. The lower-left and upper-right circulations are in the clockwise direction, the other two are in the counter-clockwise direction. The heat transfer is primarily due to conduction. Both the velocity and temperature response are synchronous with the forcing function as evident from Fig. 5.

The subsequent calculation relates to $\omega = 200$, where the flow started to be excited. In the fluid domain, there is a big clockwise rotation resulting from the combination of the two circulations existing in the upper-right and the lower-left portion of the $\omega = 450$ results and two counterclockwise circulations become small at the corners, as shown in Fig. 6. The temperature distribution displays a small slope, because of the convective effect.

As the frequency is continuously decreased to 85, the flowfield develops a strongly convective flow where small eddies start to appear in addition to the primary clockwise vortex (see Fig. 7). The point data history shows deviation from the periodicity, especially in the temperature data with a large variation which is likely caused by the strong nonlinear effect. The strongly excited flow distorted the temperature distribution and created a high gradient.

In summary, these examples are investigated by the horizontal modulation effect in zero gravity to provide the critical frequency for the transformation from conduction to convection phenomena. In addition, due to the coupling of high-mode excitation, the low-frequency case gradually creates a nonperiodic point data history.

B. Results with Thermocapillary Effect

The main purpose of this subsection is to include the surface tension effect on the free surface boundary to investigate how serious the surface tension effect appears in the flowfield. In these simulations, the Prandtl, Rayleigh, and Marangoni numbers were chosen as 7×10^{-3}, 1.771×10^{5}, and -100, respectively, in order to furnish a direct comparison with the results obtained in the previous subsection. In the first set of these computations, the cavity was subjected to vertical modulation along the direction of the temperature gradient, and the range of frequency was explored starting with $\omega = 4543$; the results of these computations are displayed in Fig. 8. Because of the combined surface tension and gravity modulation effects, it is evident that the results of Fig. 8 have one circulation instead of four main circulations as appeared in Fig. 2. The maximum stream function value is five orders bigger than the case without thermocapillarity and the values in the right portion are much larger than the left portion of the cavity (see Table 2). Apparently, the surface tension strongly dominates the flow domain even in a small Marangoni number; but due to the rectangular geometry, its effect remains primarily on the right-hand side of the cavity. Isothermal lines, owing to the thermocapillary contribution, display a convective temperature distribution in the right portion and conductive temperature distribution in the left portion, which is different from the results shown in Fig. 2. In point data history, a synchronous response is the same as having no surface tension results, but due to the influence of surface tension, the velocity data are not symmetric to the zero value as it was displayed in Fig. 2.

The next case corresponds to $\omega = 45.5$ and the results are shown in Fig. 9. Owing to the same effect of thermocapillarity, the streamlines mainly remain one big cell in the central portion, and there are two other small eddies which are opposite in directions near the walls. These two small eddies are shrunk from the two clockwise circulations, one in the upper-right portion and one in the lower-left portion (see Fig. 3); since in the $\omega = 45.5$ case the stream function strength difference between with and without surface tension results in only one order, the thermocapillary flow cannot completely expand to the whole domain (see Table 2). The isothermal lines and the point data history are similar to the case where $\omega = 4543$.

The effects of lower frequencies were probed by setting $\omega = 20$. Here, the streamlines appear with two main counter-rotating circulations in the fluid domain (see Fig. 10) which are similar to the contours shown in Fig. 4. These circulations mean the natural convection in low frequency is still dominating the fluid flow as $Ma = -100$. Because of the surface tension effect on the free surface, the time-averaged results lose their symmetric characteristic and the v velocity varies with time, shown in the point data history. When the circulation on the right-hand side has the same rotating direction as circulation created by surface tension, the surface tension provides the augmenting effect. On the other hand, when these two circulations have different rotating directions, the surface tension produces a counteracting effect.

From the preceding comparisons, it can be concluded that the natural convection flow in vertical gravity modulation is strongly influenced by the surface tension, even at a small Marangoni number. In these examples, the weak natural convection flow existing in high frequency is overcome by the thermocapillary flow; but in low frequency, the thermocapillary influence is reduced by the increase of natural convection strength.

The second set of numerical experiments at zero gravity were conducted with g modulation imposed along the direction perpendicular to the temperature gradient with thermocapillary effect. As before, we started with a relatively high value of ω and searched for the destabilizing frequency range by systematically reducing the value of this parameter. First, the example at $\omega = 450$ is investigated and the results are shown in Fig. 11. For the results without surface tension effect, the streamlines include four cells, but for the results with surface tension, the fluid flowfield is divided into two portions, the right portion with counterclockwise circulation created by thermocapillarity and the left portion with the circulation produced by natural convection. Although the two circulations occupy nearly equal area of the domain, the dif-

Table 2 Influence of finite element mesh on the solution

	Without thermocapillary effect						With thermocapillary effect, $Ma = -100$					
	$\omega = 45.5$ (vertical jitter)			$\omega = 200$ (horizontal jitter)			$\omega = 45.5$ (vertical jitter)			$\omega = 200$ (horizontal jitter)		
	Nu_h	Nu_c	Max $\lvert\psi\rvert$	Nu_h	Nu_c	Max $\lvert\psi\rvert$	Nu_h	Nu_c	Max $\lvert\psi\rvert$	Nu_h	Nu_c	Max $\lvert\psi\rvert$
15×30	2.000	2.000	0.0302	2.004	2.004	0.205	—	—	—	—	—	—
20×40	2.000	2.000	0.0244	2.005	2.005	0.245	—	—	—	—	—	—
25×50	2.000	2.000	0.0206	2.005	2.005	0.262	—	—	—	—	—	—
20×38	—	—	—	—	—	—	1.998	2.008	0.222	2.051	2.055	0.634
24×48	—	—	—	—	—	—	2.001	2.004	0.220	2.063	2.066	0.684
38×56	—	—	—	—	—	—	2.002	2.004	0.220	2.067	2.068	0.700

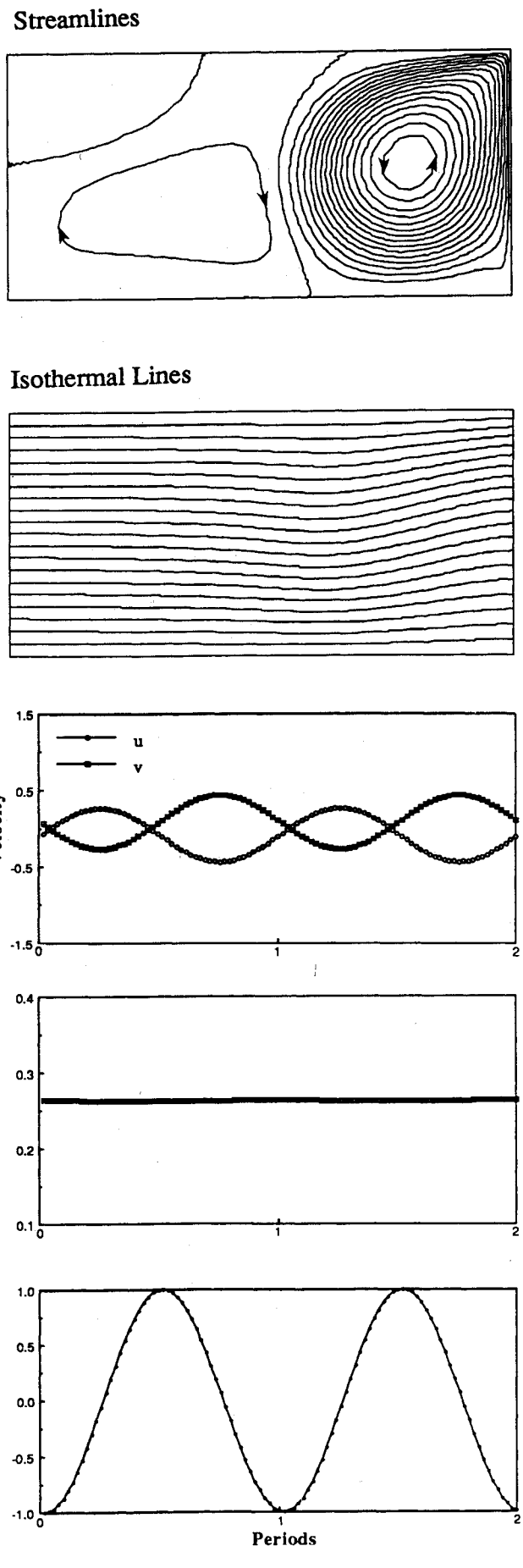

Fig. 11 Time-averaged results for $Ra = 1.771 \times 10^5$, $Ma = -10^2$, $Pr = 0.007$, $\eta = 1$, $\omega = 450$, $Ar = 0.5$, and zero g (horizontal jitter).

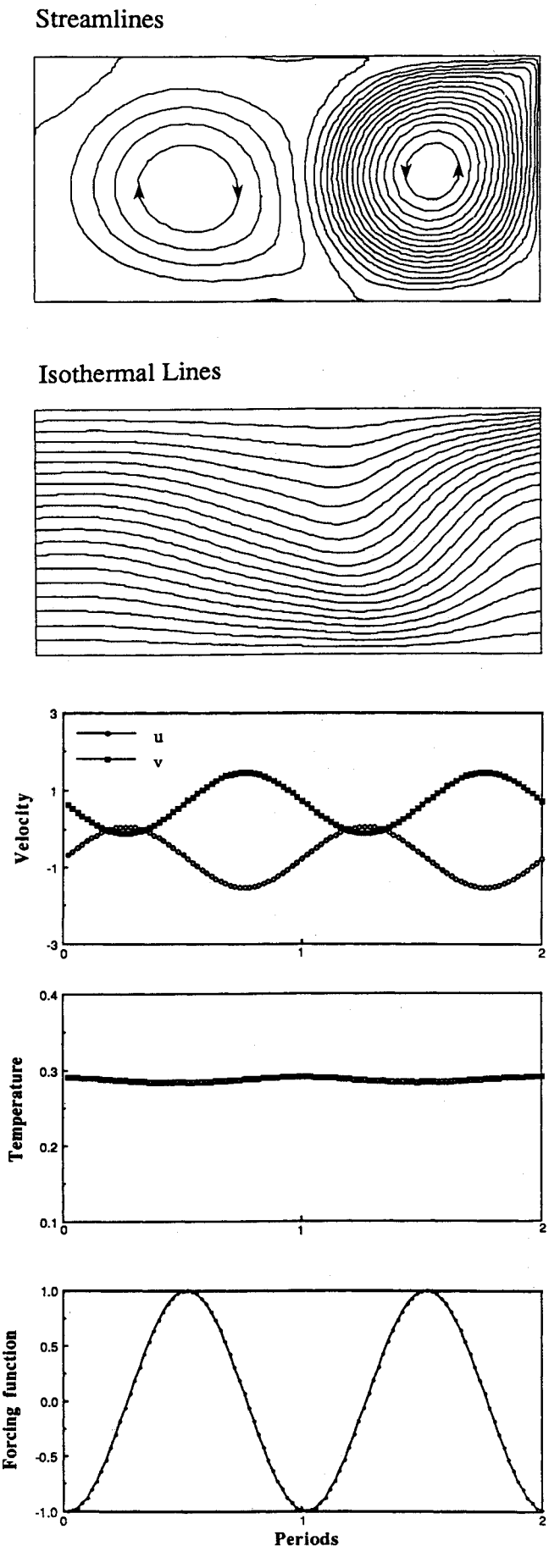

Fig. 12 Time-averaged results for $Ra = 1.771 \times 10^5$, $Ma = -10^2$, $Pr = 0.007$, $\eta = 1$, $\omega = 200$, $Ar = 0.5$, and zero g (horizontal jitter).

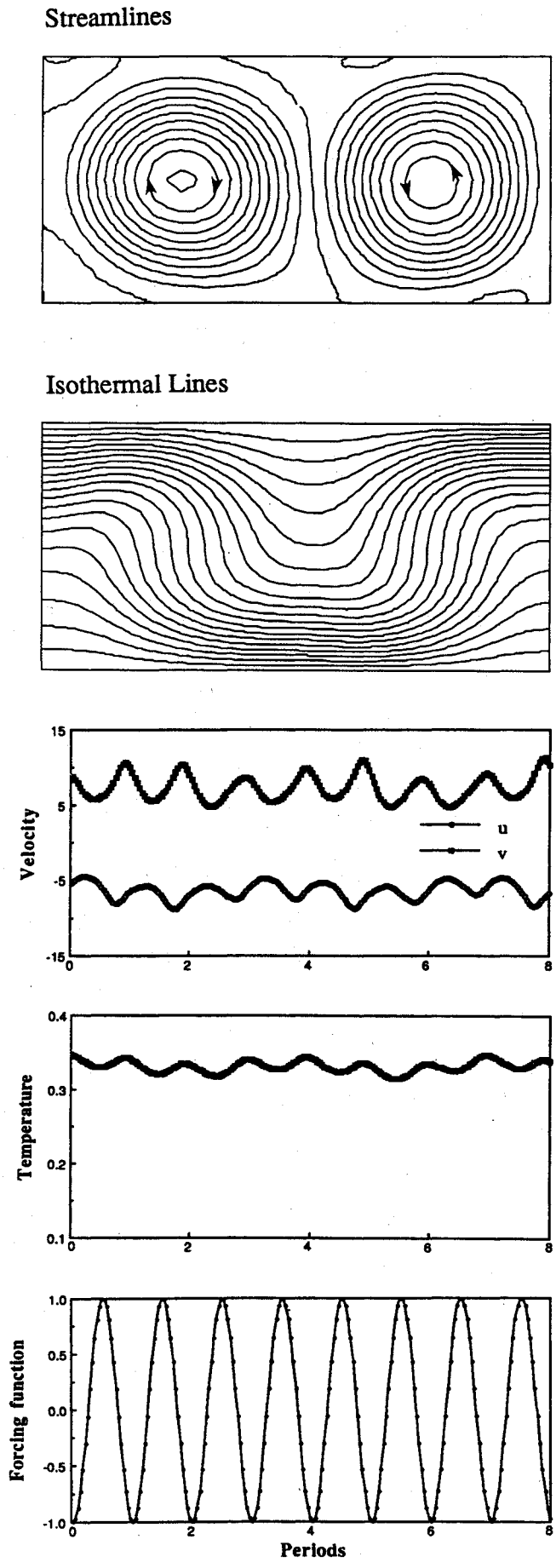

Fig. 13 Time-averaged results for $Ra = 1.771 \times 10^5$, $Ma = -10^2$, $Pr = 0.007$, $\eta = 1$, $\omega = 85$, $Ar = 0.5$, and zero g (horizontal jitter).

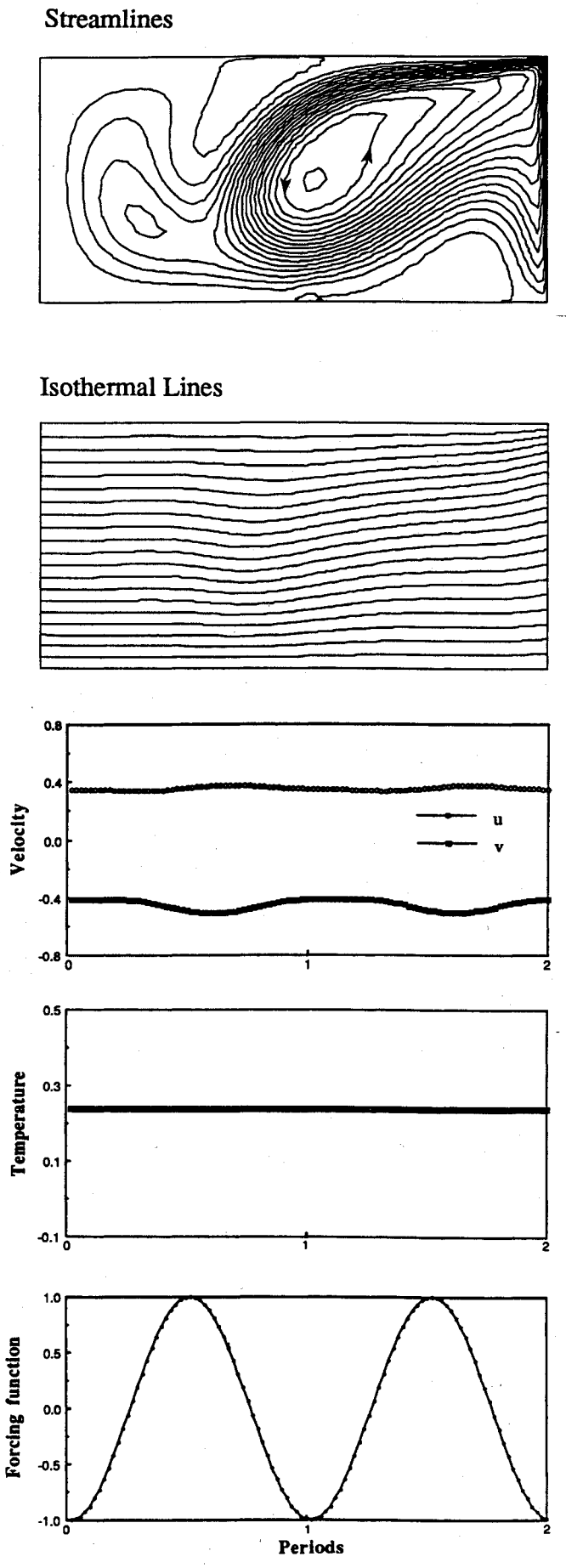

Fig. 14 Time-averaged results for $Ra = 1.771 \times 10^5$, $Ma = -10^3$, $Pr = 0.007$, $\eta = 1$, $\omega = 45.5$, $Ar = 0.5$, and zero g (vertical jitter).

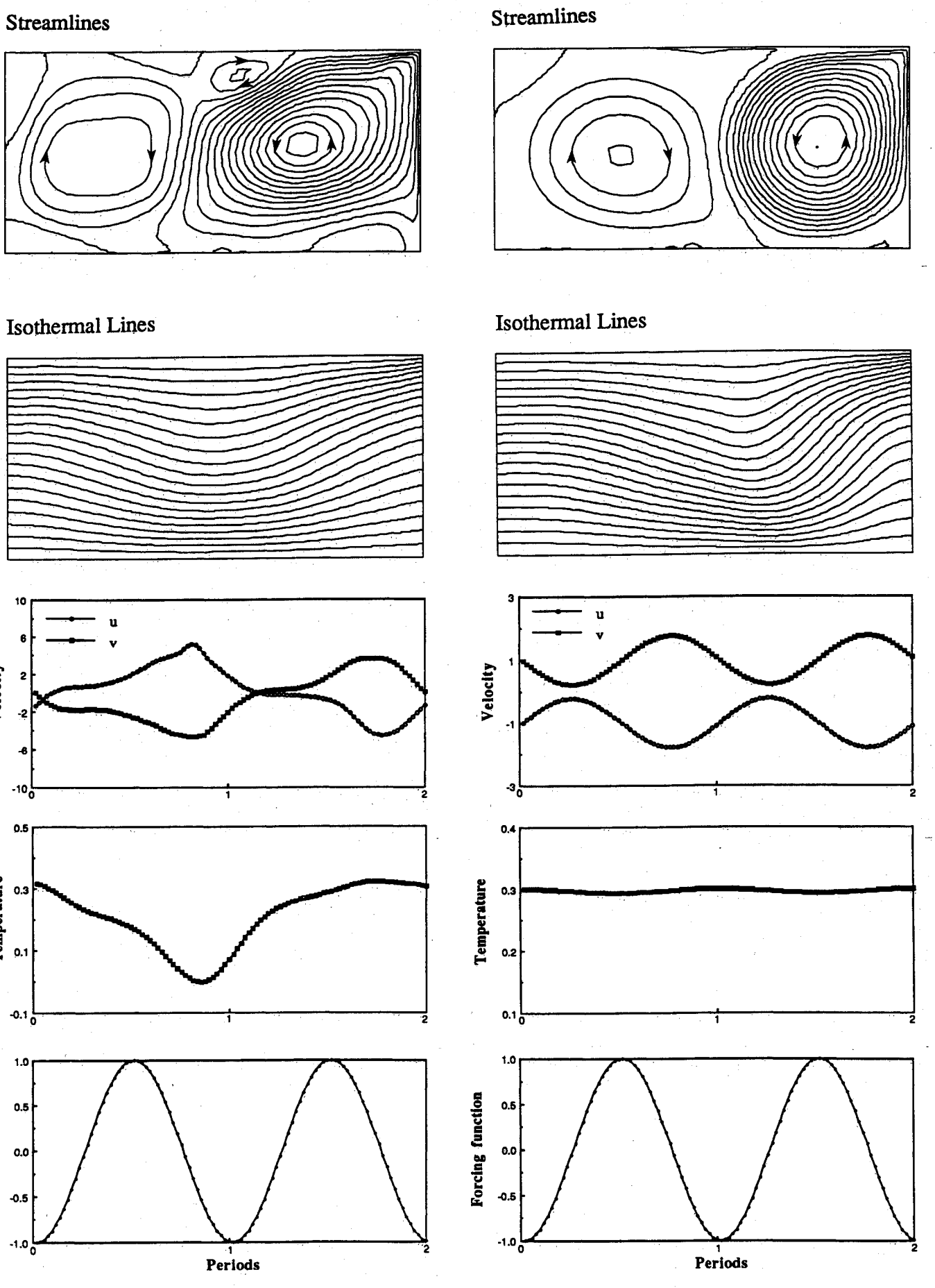

Fig. 15 Time-averaged results for $Ra = 1.771 \times 10^5$, $Ma = -10^3$, $Pr = 0.007$, $\eta = 1$, $\omega = 20$, $Ar = 0.5$, and zero g (vertical jitter).

Fig. 16 Time-averaged results for $Ra = 1.771 \times 10^5$, $Ma = -10^3$, $Pr = 0.007$, $\eta = 1$, $\omega = 200$, $Ar = 0.5$, and zero g (horizontal jitter).

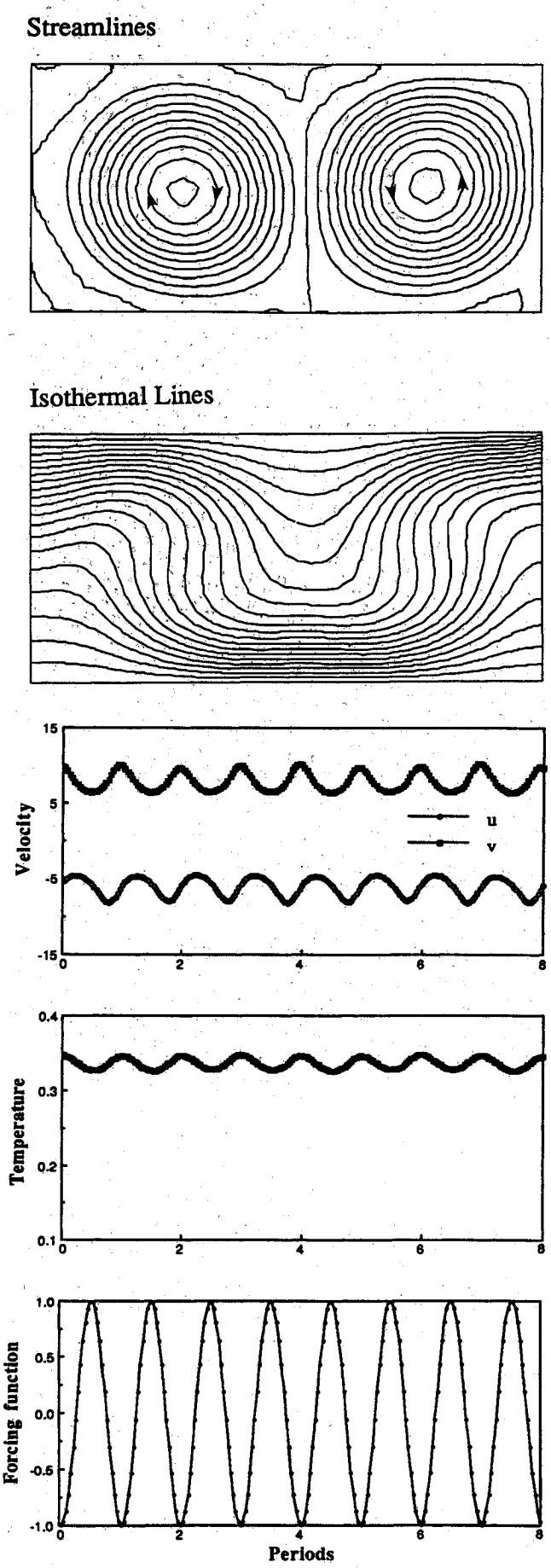

Fig. 17 Time-averaged results for $Ra = 1.771 \times 10^5$, $Ma = -10^3$, $Pr = 0.007$, $\eta = 1$, $\omega = 85$, $Ar = 0.5$, and zero g (horizontal jitter).

ference between their circulation strengths is one order. The circulation created by surface tension is still much stronger than the circulation created by the natural convectional effect. The isothermal lines display convective temperature distribution, because of the convection flowfield. The point data history displays synchronous response with more variation in the velocity.

The next case corresponds to $\omega = 200$. The streamline contours (see Fig. 12) are the same as the $\omega = 450$ results, still demonstrating a flow pattern dominated by the surface tension, which contains two big cells in the fluid domain. Comparing these two circulation strengths, we can find that they are of the same order. This means that both the natural convection and surface tension have an equal effect. Similarly, the isothermal lines demonstrate a strong convection pattern and the point data history shows synchronous response.

Finally, we did the study for the frequency $\omega = 85$. For this frequency without surface tension (see Fig. 6), the flow pattern shows a big clockwise circulation with some small eddies; and the point data history also displays a weak nonperiodic phenomenon. But with surface tension influence, the flow pattern changes to be similar to the results for $\omega = 450$ and 200 (see Figs. 11–13) displaying two counter-rotating circulations, which possess the same strength. The temperature distributions, due to the two circulations with the same order, demonstrate strong convection. However, the point data history keeps synchronous response with nonperiodic phenomena, which is the same as without surface tension results.

In addition to $Ma = -100$, we are interested in the effect of larger Ma. Therefore, some results correspond to $Ma = -1000$ are investigated. The cases include $\omega = 45.5$, 20 in the vertical gravity modulation state and $\omega = 200$, 85 in the horizontal modulation environment as listed in Figs. 14–17. The isothermal lines possess the same shape as $Ma = -100$, but the flow patterns display some difference. The circulation in streamline contours for $\omega = 45.5$ (see Fig. 14) moves closer to the central portion, and in the $\omega = 20$ case, the right circulation becomes stronger and larger (see Fig. 15). Regarding the horizontal gravity modulation cases, the difference is the increase of circulation strength in the right portion. Particularly, the increase of surface tension results in stabilizing the nonperiodic point data response for $\omega = 85$.

In summary, the surface tension effect in natural convection with horizontal gravity modulation alters the flow domain to contain two circulations simultaneously. Final solutions are obtained for each case in this subsection resulting from mutual influence between the surface tension and the natural convection effects.

V. Summary and Conclusions

In this research, a semi-implicit finite element method was applied to solve the natural convection with combined surface tension and gravity modulation effects in a rectangular cavity. For the cases without thermocapillary effect, the gravity modulation direction and frequency seriously influence the flow domain. In vertical gravity modulation, the decrease of frequency makes the point data response change from synchronous to subharmonic. For horizontal gravity modulation, the point data response transfers from synchronous to nonperiodic. However, it is common that the convective strength increases as the frequency decreases and the heat transfer mechanism changes from conduction to convection.

When the surface tension was included on the flow boundary, the physical phenomena changed dramatically. In vertical gravity modulation, the surface tension dominates the entire physical domain. In low frequency, the surface tension effect is diminished by the increase of natural convection. For horizontal gravity modulation with surface tension effect, the surface tension creates a strong circulation in the right portion which is different from the results obtained when there is no influence of thermocapillarity. But the point data history

changes from synchronous to nonperiodic which is similar to the cases where there is no surface tension effect. In conclusion, the thermocapillarity seriously influences the physical phenomena of thermal-driven cavity flow with gravity modulation in low-gravity environments.

Acknowledgments

This research was carried out with the partial support of the NSF, under Grant DMS-9112847. The computations were performed on a CRAY Y-MP at the University of Illinois, Urbana-Champaign, under Grant NSF TRA910175N. We thank reviewers for their constructive comments.

References

[1]Bergman, T. L., and Ramadhyani, S., "Combined Buoyancy- and Thermocapillary-Driven Convection in Open Square Cavities," *Numerical Heat Transfer,* Vol. 9, 1986, pp. 441–451.

[2]Bergman, T. L., and Keller, J. R., "Combined Buoyancy, Surface Tension Flow in Liquid Metals," *Numerical Heat Transfer,* Vol. 13, 1988, pp. 49–63.

[3]Carpenter, B. M., and Homsy, G. M., "Combined Buoyant-Thermocapillary Flow in a Cavity," *Journal of Fluid Mechanics,* Vol. 207, 1989, pp. 121–132.

[4]Shyy, W., and Chen, M. H., "A Study of Transport Process of Buoyancy-Induced and Thermocapillary Flow in Molten Alloy," AIAA Paper 90-0255, 1990.

[5]Keller, J. R., and Bergman, T. L., "Predication of Conjugate Heat Transfer in a Solid-Liquid System: Inclusion of Buoyancy and Surface Tension Forces in the Liquid Phase," *ASME Journal of Heat Transfer,* Vol. 111, 1989, pp. 690–698.

[6]Shyy, W., and Chen, M. H., "Interaction of Thermocapillary and Natural Convection Flows during Solidification: Normal and Reduced Gravity Conditions," *Journal of Crystal Growth,* Vol. 108, 1991, pp. 247–261.

[7]Lan, C. W., and Kou, S., "Thermocapillary Flow and Natural Convection in a Melt Column with an Unknown Melt/Solid Interface," *International Journal of Numerical Methods in Fluid,* Vol. 12, 1991, pp. 59–80.

[8]Jue, T. C., Ramaswamy, B., and Akin, J. E., "Computation of Thermocapillary and Buoyancy Affected Cavity Flow Using Semi-Implicit FEM," *Numerical Method in Thermal Problems,* Vol. 7, 1991, pp. 402–412.

[9]Incropera, F. P., Engel, A. H. H., and Bennon, W. D., "Numerical Analysis of Binary Solid-Liquid Phase Change with Buoyancy and Surface Tension Driven Convection," *Numerical Heat Transfer,* Pt. A, Vol. 16, 1989, pp. 407–427.

[10]Lacroix, M., "Effects of Buoyancy and Surface Tension Forces on the Melting of a Metal," *Numerical Heat Transfer,* Pt. A., Vol. 19, 1991, pp. 101–115.

[11]Gresho, P. M., and Sani, R. L., "The Effects of Gravity Modulation on the Stability of a Heat Fluid Layer," *Journal of Fluid Mechanics,* Vol. 40, 1970, pp. 783–806.

[12]Kamotani, Y., Prasad, A., and Ostrach, S., "Thermal Convection in an Enclosure Due to Vibrations Aboard Spacecraft," *AIAA Journal,* Vol. 19, No. 4, 1981, pp. 511–516.

[13]Biringen, S., and Danabasoglu, G., "Computation of Convection Flow with Gravity Modulation in Rectangular Cavities," *Journal of Thermophysics and Heat Transfer,* Vol. 4, No. 3, 1990, pp. 357–365.

[14]Ramaswamy, B., Jue, T. C., and Akin, J. E., "Finite Element Analysis of Oscillatory Flow with Heat Transfer Inside a Square Cavity," *AIAA Journal,* Vol. 30, No. 2, 1992, pp. 412–422.

[15]Jue, T. C., "Numerical Study of Cavity Natural Convection with Augmenting and Counteracting Effects by Projection Finite Element Method," Ph.D. Thesis, Rice Univ., Houston, TX, 1992.

[16]Zehr, R. L., Chen, M. M., and Mazumder, J., "Thermocapillary Convection of a Differentially Heated Cavity at High Marangoni Numbers," National Heat Transfer Conf., Paper 87-HT-29, Pittsburgh, PA, 1987.

[17]Knabe, W., and Eilers, D., "Low Gravity Environments in Space Lab," *Acta Astronautica,* Vol. 9, No. 4, 1982, pp. 182–198.

Earl A. Thornton
Associate Editor